# The Effect of Heat Transfer on Local Solidification Kinetics of Eutectic Al-Si Cast Alloy

*C. González-Rivera, H. Cruz M., A. García H., and J.A. Juarez-Islas*

*(Submitted 12 May 1998; in revised form 15 September 1998)*

**Recently, Fourier thermal analysis (FTA) has been proposed as a suitable technique to obtain information about local solidification kinetics in casting alloys. In this work, FTA was applied to a near-eutectic aluminum-silicon cast alloy in order to seek experimental evidence supporting the solidification kinetics obtained from this method. Also, a heat-transfer/solidification-kinetics model was used to compare predictions with experimental results. The metallographic findings, focused on interlamellar eutectic spacings in different locations within a cylindrical casting, support the solidification kinetics obtained from FTA. The model and experimental outcome including FTA results and metallographic observations suggest that local solidification kinetics depend strongly on local heat transfer, and the analysis of this dependence may be used to explain the observed changes in microstructural characteristics at different locations within castings.**

**Keywords** Al-Si eutectic, Fourier thermal analysis, interlamellar eutectic spacings, solidification kinetics

## 1. Introduction

The modeling of solidification has recently received considerable attention and has included among other topics the modeling of kinetics of microstructure formation coupled to macroscopic heat flow (Ref 1). The main reasons behind this attention are the potentially significant savings in the time required for prototyping and in the cost associated with defective castings (Ref 2). However, despite the recent advances in microstructure formation modeling (Ref 1-4), there are only a limited number of studies (Ref 5-8) directed toward the analysis of local solidification kinetics as it is influenced by the heat transfer process involved in casting. During solidification, the temperature gradients existing in the casting give rise to inhomogeneous volume fraction of solidified phases (Ref 5) and to the presence of different microstructural characteristic lengths at different locations within the casting (Ref 6).

In order to predict the solidification kinetics of an alloy at any location within castings, the Fourier heat transfer equations have been included (Ref 5, 8) in the mathematical modeling of solidification processes, enabling the investigation of the temperature-gradient effects on the solidification behavior of cast products.

The verifications between model predictions and experimental results can be properly addressed by using Fourier Thermal Analysis (FTA) (Ref 5, 7). Because this method is based on measurements of the actual thermal field of the liquid metal during solidification, it is expected to be reliable in its predictions with regard to the solidification kinetics data that result from the numerical processing of the temperature measurements in two locations within a symmetric casting. The fundamental concepts and implementation of this method have been described elsewhere (Ref 7).

The purpose of this work is:

- To seek experimental evidence supporting the solidification kinetics obtained from Fourier thermal analysis in an eutectic aluminum-silicon sand cast alloy
- To use a heat-transfer/solidification-kinetics model to predict the local solidification kinetics in order to compare predictions with experimental results
- To analyze the information obtained in order to explore the effect of heat transfer on the local solidification kinetics within castings

## 2. Experimental Procedure

The experimental array employed in this work is represented schematically in Fig. 1. Preweighted quantities of a

**Nomenclature**

| | |
|---|---|
| $C_p$ | Volumetric specific heat, J/m$^3$ · °C |
| $k$ | Thermal conductivity, W/m · °C |
| $\varphi$ | Density, kg/m$^3$ |
| $T$ | Temperature, °C |
| $t$ | time, s |
| $r$ | Radial position, m |
| $L_f$ | Volumetric latent heat, J/m$^3$ |
| $Q_a$ | Volumetric heat accumulation flow, W/m$^3$ |
| $Q_c$ | Volumetric heat dissipation flow, W/m$^3$ |
| $Q_s$ | Volumetric latent heat generation flow, W/m$^3$ |
| $h$ | Convective heat transfer coefficient, W/m$^2$ · °C |
| $\hat{N}_E$ | Volumetric grain density, m$^{-3}$ |
| $\Delta T_E$ | Eutectic undercooling, °C |

C. González-Rivera, H. Cruz M., and A. García H., Fac. de Quimica, Departamento de Metalurgia, Circuito Exterior S/N, Cd. Universitaria, 04510, Mexico, D.F., Mexico, and J.A. Juarez-Islas, Instituto de Investigaciones en Materiales, Departamento de Materiales Metalicos y Ceramicos, Circuito Exterior S/N, Cd. Universitaria, 04510, Mexico, D.F., Mexico.

near-eutectic aluminum-silicon alloy, designated as A1 alloy, and whose composition is shown in Table 1, were melted in a resistance furnace under an argon atmosphere. The alloy was degassed with argon during the 8 min prior to pouring and directly cast into a green sand mold with a cylindrical casting cavity of 0.016 m of internal diameter and 0.15 m in height (with an insulated top and bottom). In order to record the thermal history of the alloy during cooling, two 0.0003 m diam bore, type K thermocouples, with alumina sheath, 0.0016 m outside diameter, were introduced at the mid-height of the sand mold cavity at two different distances from the center of the casting. Thermocouple outputs were recorded on a personal computer with data recording and processing facilities. The cooling curves obtained were numerically processed using the FTA method (Ref 7) in order to obtain information about the solidification kinetics of the region of the casting near the inner thermocouple.

After solidification, the specimen was cut in half in order to verify the positions of the thermocouples, and a cross section of the specimen was polished for microstructural observation. Three zones of interest were considered during metallographic examinations of the cross section of the cylindrical probe: (1) center of the probe, at $r = 0$ m, (2) edge of the probe, at $r = 0.008$ m, and (3) intermediate region, at $r = 0.004$ m. Attention was focused on the average interfacial distances between eutectic lamellae.

### 2.1 *Heat-Transfer/Solidification-Kinetics Model*

**Heat Transfer.** During the cooling and solidification of the aluminum-silicon alloy in sand molds, it is assumed that the macroscopic heat flow is governed by conductive heat transfer and latent heat generation due to solidification (i.e., convective effects are not considered). Then the energy balance applied to the metal/mold system can be written as:

**Table 1 Chemical composition of alloy A1**

| | Composition, wt% | | | | | | |
|---|---|---|---|---|---|---|---|
| Alloy | Si | Fe | Cu | Mn | Mg | Zn | Al |
| A1 | 11.43 | 0.51 | 0.62 | 0.19 | 0.10 | 0.05 | bal |

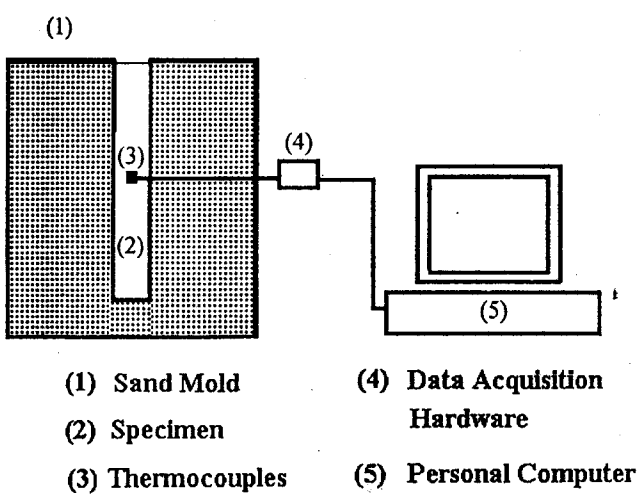


**Fig. 1** Schematic representation of the experimental array

$$C_{p_i}\frac{\partial T(x,t)}{\partial t} = \nabla[k_i \nabla T(x,t)] + L_f\frac{\partial f_s(x,t)}{\partial t} \quad \text{(Eq 1)}$$

where $T(x,t)$ is the temperature field, $t$ is the time (seconds), $x$ is the position, $C_p$ is the volumetric specific heat, $k$ is the thermal conductivity, $L_f$ is the volumetric heat of fusion, $f_s(x, t)$ is the solid fraction, and the subscript $i$ indicates the metal domain ($i = 1$) or the mold domain ($i = 2$). The term involving $f_s(x,t)$ is null except for the metal domain during solidification. Assuming temperature independence of the thermal conductivity and that there is not heat flux in the $\theta$ and $Z$ directions for a cylindrical system, Eq 1 reduces to:

$$C_{p_i}\frac{\partial T(r,t)}{\partial t} = k_i\frac{1}{r}\frac{\partial}{\partial r}\left(r\frac{\partial T(r,t)}{\partial r}\right) + L_f\frac{\partial f_s(r,t)}{\partial t} \quad \text{(Eq 2)}$$

$$Q_a = Q_c + Q_s$$

where $r$ is the radial position within the system, and the terms $Q_a$, $Q_c$, and $Q_s$ are the volumetric heat accumulation flow, the volumetric heat dissipation flow, and the volumetric latent heat flow, respectively. To solve Eq 2 $f_s(r, t)$, the solid fraction as a function of time and position within the casting, must be described. This information is provided by the solidification kinetics model coupled to the heat-transfer calculations.

In this work, it is assumed that no thermal impedance exists at the interface between the mold and the casting (i.e., the air gap formation has not been considered). Also, it is assumed that there is a convective heat transfer at the external mold surface and an instantaneous filling of the mold cavity. Accordingly, the following boundary and initial conditions were used to solve Eq 2:

Metal/mold interface: $$k_m\frac{\partial T}{\partial r} = k_s\frac{\partial T}{\partial r} \quad \text{(Eq 3a)}$$

External mold surface: $$k_s\frac{\partial T}{\partial r} = h(T_{s,Rt} - T_\infty) \quad \text{(Eq 3b)}$$

where $h$ is the convective heat transfer coefficient at the external mold surface, and the subscripts m, s, and Rt refer to the metal, the sand mold, and the external surface of the mold, respectively. The initial conditions that were considered during the simulation are the pouring temperature, $T_p$, for the metal domain and the room temperature, $T_\infty$, for the mold domain.

In order to solve Eq 2, a discretized description of the cylindrical metal/mold system is generated in the form of a finite difference mesh, composed of a known number of cylindrical volume elements (VE). When $i = 1$ (i.e., metal domain) and during solidification, the thermal history of a VE can be obtained from the evolution of the local heat flow accumulation term, $Q_a$ (see Eq 2), which in turn can be simulated through the knowledge of the net heat exchange of the VE to its surroundings, $Q_c$, and of the latent heat released as a result of local

solidification, $Q_s$, during the computing time step. Rearranging Eq 2 for the metal domain:

$$\frac{\partial T(r,t)}{\partial t} = \frac{\alpha_m}{r}\frac{\partial}{\partial r}\left(r\frac{\partial T(r,t)}{\partial r}\right) + \frac{Q_s}{C_p} = ZF + \frac{Q_s}{C_p} \quad \text{(Eq 4)}$$

where $\alpha_m$ is the thermal diffusivity of the metal, and $ZF$ is the Fourier zero curve or baseline, which can be calculated, for symmetric temperature fields (Ref 7), by using the thermocouple readings at two positions within the casting:

$$ZF = \alpha_m\left[\frac{4(T_2 - T_1)}{r_2^2 - r_1^2}\right] = \frac{Q_c}{C_p} \quad \text{(Eq 5)}$$

In Eq 5, $r$ is the radial position, relative to the symmetry axis of the casting, the subscripts 1 and 2 refer to the inner and the outer thermocouple positions within the casting, respectively, and $Q_c$ represents the net volumetric heat flow exchanged by the central region of the casting (the region situated between the symmetry axis, $r = 0$ and $r_m = (r_1 + r_2)/2$) to the surroundings. Equation 6, obtained by rearranging Eq 4 in terms of $Q_s$, shows that during solidification, the instantaneous volumetric latent heat liberated in the central region of the casting can be calculated from the difference between the cooling rate, measured at the inner thermocouple position and the $ZF$ baseline curve:

$$Q_s = C_p\left(\frac{\partial T_1}{\partial t} - ZF\right) \quad \text{(Eq 6)}$$

Equation 6 can be seen as the first step of the generation, by FTA, of solidification kinetics information. A detailed description of the numerical processing of the cooling curves in order to obtain quantitative information on solidification kinetics is given in Ref 7.

**Solidification Kinetics.** The model assumes instantaneous nucleation of the equiaxed eutectic grains and uses a simple empirical nucleation law that correlates the number of eutectic nuclei and the cooling rate by employing a parabolic equation of the form:

$$\hat{N}_E = A + B\left(\frac{\partial T}{\partial t}\right)^2_{T=T_E} \quad \text{(Eq 7)}$$

were $\hat{N}_E$ is the nucleation site density. The constants $A$ and $B$ are shown in Table 2 and were determined experimentally from grain density (number/m$^3$) versus cooling rate data. Those data were obtained by measuring the numbers of grains by the mean intersection method on several probes of A1 alloy cooled at different cooling rates and by linking—by numerical regression—the eutectic grain density to the cooling rate data when the probe achieved the eutectic temperature of the alloy (Ref 9).

The eutectic grains are assumed to be spherical in shape, and the rate of growth of eutectic grains is calculated using the relationship:

$$\frac{\partial R_E}{\partial t} = \mu_E \Delta T_E^2 \quad \text{(Eq 8)}$$

where $R_E$ is the radius of the eutectic growing grains, $\mu_E$ is the eutectic growth constant, and $\Delta T_E$ is the eutectic undercooling, $\Delta T_E = T_E - T$. Calculations were performed using $\mu_E = 5 \times 10^{-6}$ (m/s · °C$^2$) (Ref 1).

The effect of grain impingement on the solidified volume is taken into account by using the Johnson-Mehl (Ref 9) approximation to describe the solid fraction:

$$f_s = 1 - \exp\left(-(4/3)\,\pi\,\hat{N}_E\,R_E^3\right) \quad \text{(Eq 9)}$$

Furthermore, in order to enhance the simulated cooling curve fitting relative to experimental results near the end of freezing, the growth rate of the eutectic microconstituent is slowed (Ref 10) by the factor $(1 - f_s)$.

The coupling between macroscopic heat flow and solidification kinetics models was achieved by using a fully two-way coupling, as described by Sasikumar (Ref 11).

Equation 2 was solved by the implicit finite difference method. During solidification, the local changes in the fractions of solid within the casting are calculated at the beginning of every interval of time by inputting the temperature field at this time into the solidification kinetic model. The results obtained are then used during the calculation of the next temperature field.

This model was used to generate simulated cooling curves in the conditions corresponding to the experimental measurements. The thermophysical data used during calculations are shown in Table 2.

**Table 2 Selected data used during simulation**

| | |
|---|---|
| **Nucleation and growth constants (metal)** | |
| $A = 5.21 \times 10^8$ | m$^{-3}$ |
| $B = 3.56 \times 10^6$ | s$^2$/m$^3$ · °C$^2$ |
| $\mu_E = 5 \times 10^{-6}$ | |
| **Thermal conductivity (metal)(a)** | |
| $k_l = 77.36$ | W/m · °C |
| $k_s = 122.26$ | W/m · °C |
| **Thermal diffusivity (metal)(a)** | |
| $\alpha_l = 3.19 \times 10^{-5}$ | m$^2$/s |
| $\alpha_s = 5.5 \times 10^{-5}$ | m$^2$/s |
| $\varphi = 2450$ | kg/m$^3$ |
| $L_f = 9.5 \times 10^8$ | J/m$^3$ |
| **Sand mold** | |
| $\varphi = 1500$ | kg/m$^3$ |
| **Thermal conductivity (mold)** | |
| $k = -5.54 \times 10^{-10} T^3 + 1.88 \times 10^{-6} T^2 - 1.48 \times 10^{-2} T + 1.35$ | W/m · °C |
| **Heat capacity (mold)** | |
| $T > 600$ °C $C_p = -9.51 \times 10^{-3} T^2 + 1.19\,T + 740.69$ | J/kg · °C |
| $T < 600$ °C $C_p = 1045.03 + 0.13\,T$ | J/kg · °C |
| $h = 20$ | W/m$^2$ · °C |

(a) Subscripts: l, liquid; s, solid

## 3. Results and Discussion

The pouring temperature of the experimental alloy and the thermocouple locations are shown in Table 3. The resulting cooling curves ($T$ versus $t$) for the inner and outer thermocouple positions, obtained during the cooling and solidification of the A1 alloy are shown in Fig. 2 and the predicted cooling curves according to the solidification model are shown in Fig. 3.

In order to obtain local solidification kinetics information—related to the metal region near the inner thermocouple—using the experimental data, the experimental cooling curves were numerically processed using the Fourier method (Ref 7). The simulated cooling curves were also treated using this method. The results obtained are shown in Fig. 4 to 8.

The cooling curve derivatives ($dT/dt$) for the thermocouple positioned at $r_1$ of Fig. 2 and 3 corresponding to the experimental and predicted curves, respectively, are shown in Fig. 4, including the thermal analysis baselines for zero Fourier ($ZF$, Eq 5), once again, of the experimental and predicted cooling curves. The trend and shape of both parameters ($dT/dt$ and $ZF$) show a very close resemblance with the results obtained from FTA processing of cooling curves associated to other eutectic system alloys, in particular for eutectic gray cast iron (Ref 5, 7).

The solidification rates obtained from the FTA method show an initial maximum of a relatively small magnitude followed by a significantly larger second maximum, attained almost at the end of solidification (Fig. 5). The experimental and predicted solid fractions in the central region of the casting, obtained from FTA, are shown in Fig. 6. Regarding Fig. 5 and 6, at the initial stage of solidification, the relatively slow operating solidification rate produces a slow solid fraction increment that shows an initial restriction for solidification development in the central part of the casting. This restriction is progressively eliminated as the solidification of the cast reaches the end.

**Table 3 Experimental conditions and thermocouple locations**

| Alloy | Pouring temperature, °C | Thermocouple locations | |
|---|---|---|---|
| | | $r_1$, m | $r_2$, m |
| A1 | 680 | 0.0005 | 0.004 |

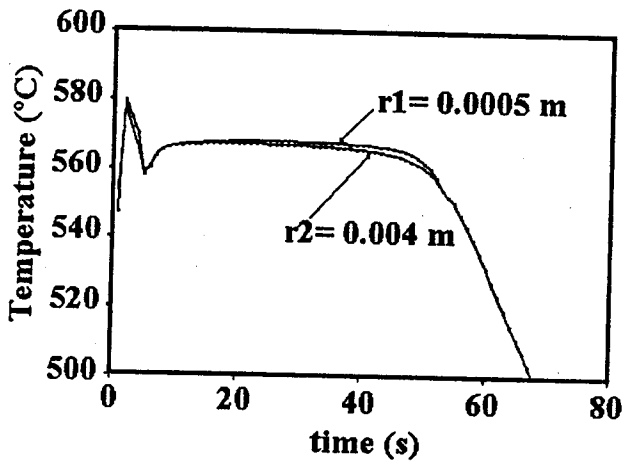


Fig. 2 Experimental cooling curves at the locations of interest, shown in Table 3

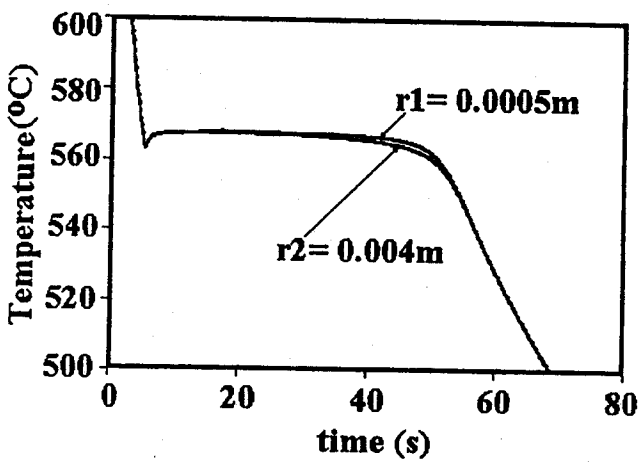


Fig. 3 Predicted cooling curves at the locations of interest, shown in Table 3

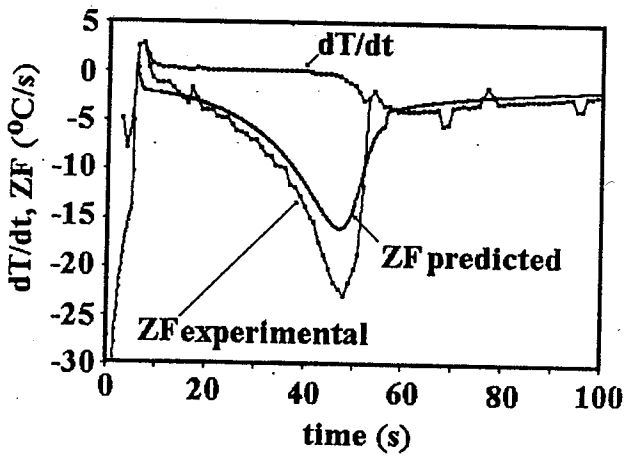


Fig. 4 Experimental and predicted temperature derivatives, and $ZF$ thermal baselines at the center of the eutectic Al-Si bar using FTA

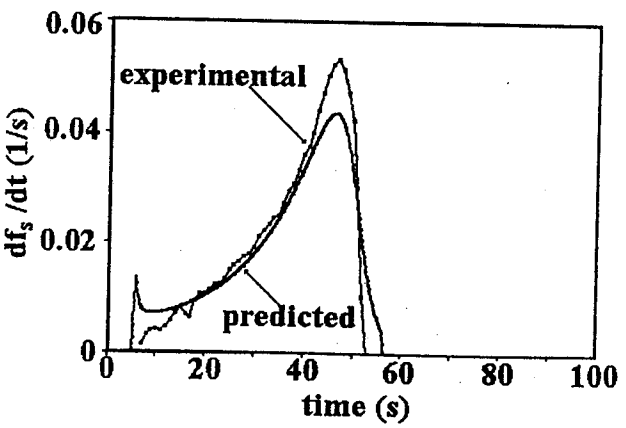


Fig. 5 Experimental and predicted solidification rates at the center of the eutectic Al-Si bar using FTA

Figure 7 shows the solid fraction and derivative cooling-curve evolution obtained from FTA processing of experimental cooling curves. Here, it can be observed that the last liquid solidifying in the central part of the casting solidifies under a more negative cooling rate promoting large undercooling in this zone. Accordingly, Fig. 8 shows the experimental solid fraction obtained from FTA and the apparent eutectic undercooling (Ref 12) as a function of time. The eutectic growth theories (Ref 13, 14), based on experimental evidence, indicates that an increment in the operating undercooling during solidification promotes a finer eutectic microstructure, with narrow spacings between eutectic lamellae. Hence, FTA results indicate the presence, in the thermal center of the casting, of a liquid metal that solidifies under an increasing degree of undercooling, and this in turn implies the presence in this zone of fine and narrowly spaced eutectic silicon flakes. Metallographic findings confirm the presence, at the thermal center of the casting, of a eutectic microstructure that shows very narrow interfacial distances between eutectic lamellae, as shown in Fig. 9, which presents the interlamellar spacings in the central region near the symmetry axis of the casting (Fig. 9a), the external region near the metal/mold interface (Fig. 9b), and in the intermediate region (Fig. 9c).

Similar effects have been shown by other eutectic alloy systems. In eutectic gray cast iron (Ref 6, 15), the presence of microstructural length refinement in the region near the thermal center of the casting has been explained as an effect of the increasing degree of undercooling in the final solidifying liquid metal.

In order to gain more insight into the factors affecting the solidification kinetics within the casting, it is interesting to explore the process phenomenology through the examination of the interdependence existing between the various features associated with the solid-fraction evolution in different locations within the metal as revealed by the model.

Figure 10 shows the solidification model predictions for the local solidification rates and the volumetric heat flow dissipated, $Q_c$, as a function of time considering three positions inside the casting. Here (c) refers to the symmetry axis of the cylinder, $r = 0$ m, (i) to the metal/mold interface, $r = 0.008$ m, and (m) to the intermediate region situated at $r = 0.004$ m. Note that the relative positions within the melt clearly affect the local evolution of solidification rates and the thermal events. This in turn modifies the local conditions during solidification and affects the microstructural characteristics of the solid formed at different positions within the casting.

Figure 10 also shows a very close dependence of the solidification evolution on the local heat transfer. As $Q_c$ represents the heat flux exchanged from the local volume to its surroundings, the model outcome indicates that local solidification depends on the possibility of latent heat extraction from the local volumes to the external zones of the system. This in turn is restricted by the low heat extraction capacity of the sand mold. It is a well-known fact that the heat extracted from the casting is controlled by the low thermal diffusivity of the sand mold (Ref 16). The amount of heat that can be transferred through the mold imposes a dynamical restriction on the cooling kinetics of the casting.

During the cooling process, when the region near the metal/mold interface reaches the eutectic temperature, local solidification starts. Because the latent heat generated cannot be easily transferred to the mold, due to the restrictions mentioned above, the heat accumulation in this region produces changes in the thermal gradients acting within the casting.

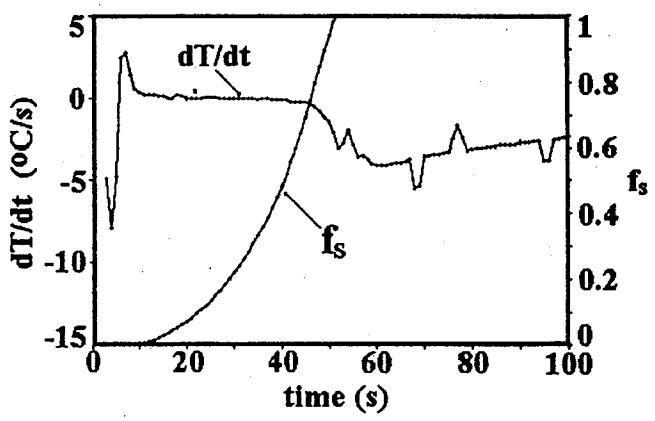


Fig. 7 Derivative of the experimental cooling curve and volume fraction of solidified Al-Si near-eutectic alloy at the center of the rod casting using FTA

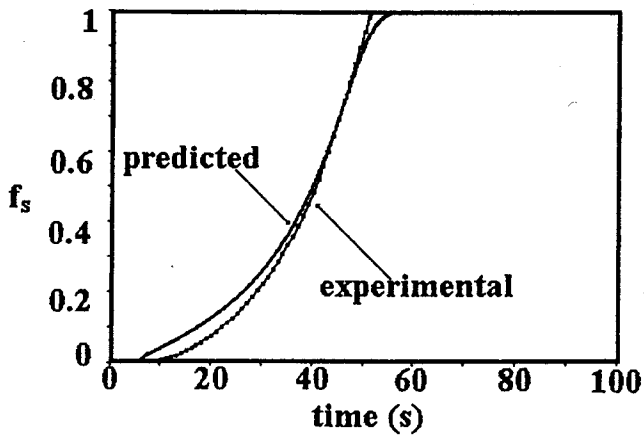


Fig. 6 Experimental and predicted volume fractions of solidified Al-Si eutectic alloy at the center of the rod casting using FTA

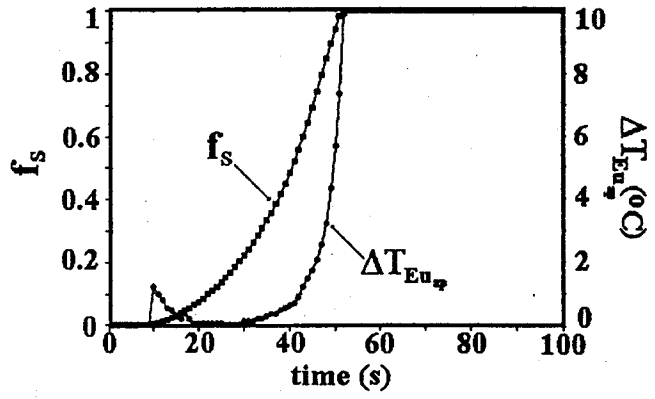


Fig. 8 Experimental volume fraction of solidified Al-Si eutectic alloy and apparent eutectic undercooling in the central region of the casting

Figure 11 shows the solidification model predictions for the local solidification rates and the local thermal gradients as a function of time in the casting regions discussed previously. A closer examination of the results shown in Fig. 11 indicates that, when the outer casting zone, (i), starts its solidification and as the latent heat cannot be easily transferred to the mold, then the local heat accumulation produces a reduction of the local thermal gradients acting on the inner regions (m) and (c). This in turn modifies the heat exchanges between the different regions of the casting ($Q_c$ in Fig. 10) and controls the solidification evolution within the casting. Thus, the latent heat liberated during the eutectic solidification of the outer zones and the heat extraction rate imposed by the low thermal diffusivity of the mold are related to the changes observed in the local thermal gradients in the casting, which restrict the solidification of the inner zones by controlling the amount of heat that can be transferred from the inner casting regions to the outside.

Model predictions show that the solidification process starts almost at the same time in all the regions of the casting, as revealed by the sudden increase in the solidification rates, corresponding to the three casting positions (see Fig. 10, at $t = 6$ s). After the start of solidification, there exists a hindering effect, related to the local thermal gradient changes, that slows the solidification rates acting in the inner zones of the casting, and this trend continues until most of the heat liberated by the solidification of the outer zone is dissipated through the metal/mold interface. When this is achieved, the inner regions

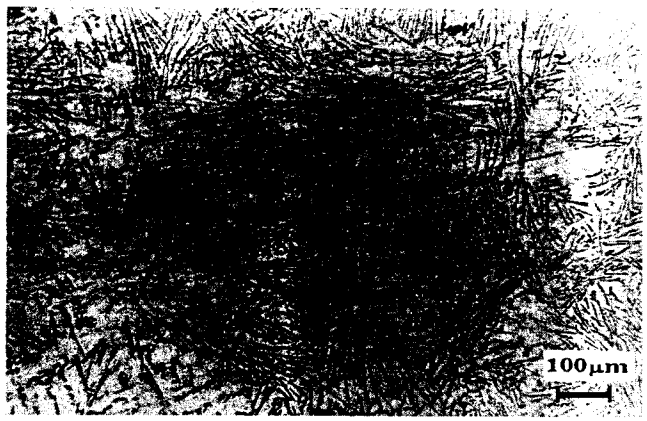


(a)

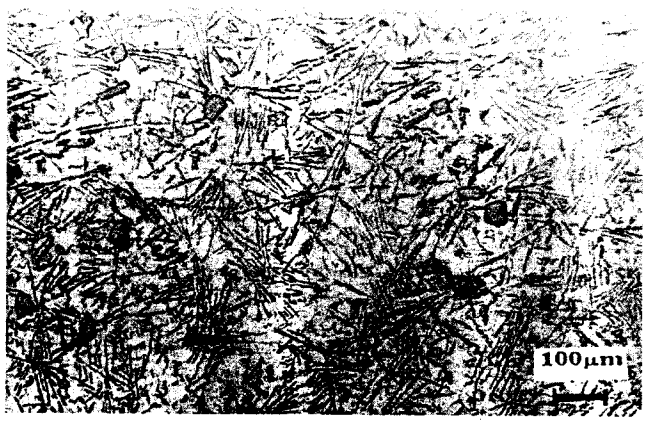


(b)

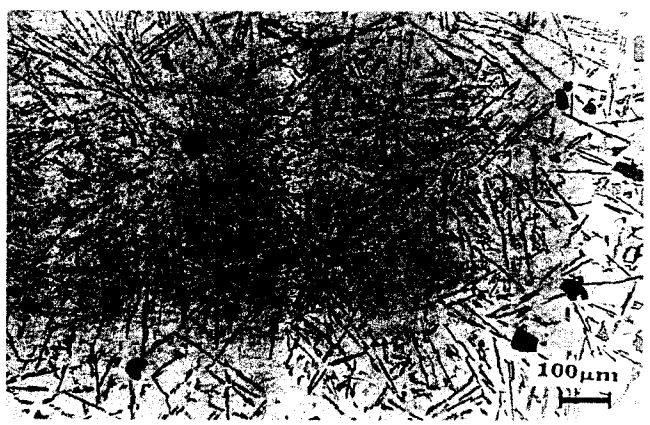


(c)

**Fig. 9** Interlamellar spacings in different positions of the test casting. (a) central region, $r = 0$ m. (b) External region, $r = 0.008$ m. (c) Intermediate region, $r = 0.004$ m

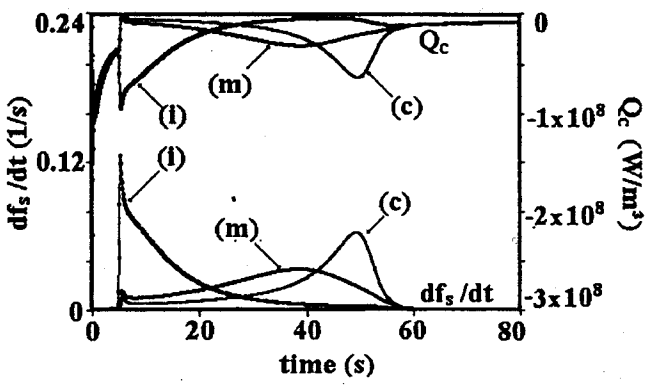


**Fig. 10** Solidification rates and volumetric heat flow dissipated, $Q_c$, as a function of time and position inside the casting, predicted by the model. (c) refers to the region near the symmetry axis of the cylinder, $r = 0$ m; (i) to the metal/mold interface, $r = 0.008$ m; and (m) to the intermediate region situated at $r = 0.004$ m.

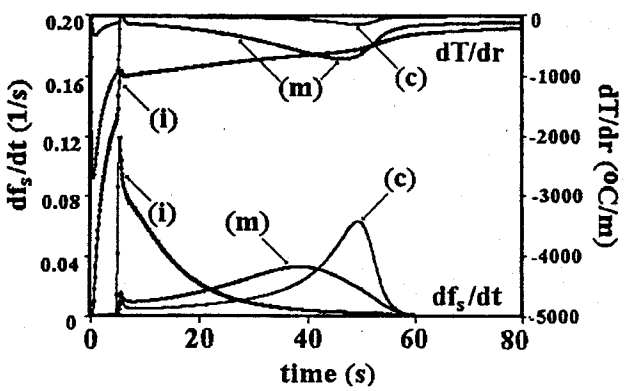


**Fig. 11** Solidification rates and local thermal gradients as a function of time and position inside the casting predicted by the model. (c) refers to the region near the symmetry axis of the cylinder, $r = 0$ m; (i) to the metal/mold interface, $r = 0.008$ m; and (m) to the intermediate region situated at $r = 0.004$ m.

accelerate its solidification by increasing sequentially its solidification rates. Furthermore, the relative magnitude of the maximum local solidification rates indicates that the undercoolings acting when solidification develops more intensively in the external and in the central region of the casting are larger than those present during the solidification of the intermediate region of the casting. This implies finer interlamellar spacings at the edge and in the center of the casting than those present in the intermediate region, as shown by the metallographic examination of the test probe (see Fig. 9).

Figure 12 shows the solid fraction and the eutectic undercooling evolution of the external and central region of the casting predicted by the model. In this figure, it can be seen that the last liquid alloy in the central region solidifies with an increasing degree of undercooling. This shows that the model predictions follow the experimental findings. The presence, at the thermal center of the casting, of a liquid alloy that can achieve considerable undercooling during the last stages of solidification can be explained as a result of the evolution of internal thermal gradients during the solidification process. This in turn can be the reason behind some phenomena that have been encountered in other alloy systems, specifically the occurrence of secondary nucleation (Ref 6) and the effect called inverse chill in gray irons.

With regard to the simplified assumptions used in this work, the roll of fluid flow and of the air gap formation on the effects discussed above must be established. It is thought that the presence of an air gap promotes the mentioned effects.

Finally, the model and experimental results, including FTA results and metallographic observations, suggest that there is a strong dependence of local solidification kinetics on local heat transfer, and the analysis of this dependence may be used to explain the observed changes of microstructural characteristics at different locations within castings.

## 4. Conclusions

Fourier thermal analysis, applied to the experimental cooling curves obtained under the conditions present in this work, indicates the presence, in the thermal center of the casting, of a liquid alloy that solidifies under an increasing degree of undercooling at the end of casting solidification. This in turn implies the presence in this zone of fine and narrowly spaced eutectic silicon flakes. Metallographic findings confirm the presence, at the thermal center of the casting, of an eutectic microstructure that shows very narrow interfacial distances between eutectic lamellae. This supports the solidification kinetics obtained from FTA.

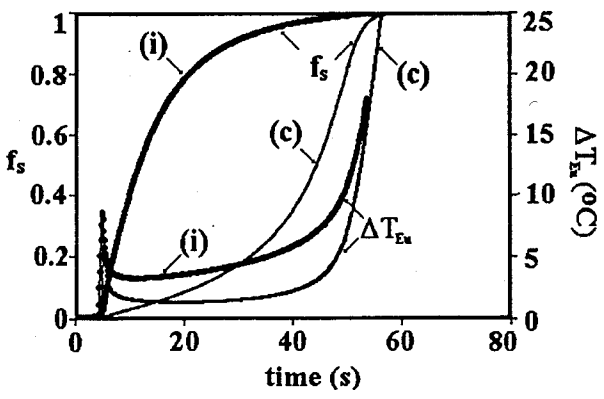


**Fig. 12** Predicted volume fractions of solidified Al-Si eutectic alloy and eutectic undercoolings in the central, (c), and external, (i), regions of the casting

Comparing the FTA results corresponding to experimental data with those associated with the simulation solidification model used in this work, one can observe a close resemblance between the shape of the experimental cooling curves, derivatives of the cooling curves, thermal analysis baselines, solid fraction evolution, and solidification rates with those obtained from the Fourier analysis of the predicted cooling curves. Thus, the computer simulation predictions are in good agreement with the experimental results.

During solidification of eutectic cast aluminum-silicon unmodified alloys, the characteristic microstructural lengths depend on the position in the cylindrical casting. The observed trend is as follows: very narrow interlamellar spacings at the edge of the casting followed by an intermediate zone showing coarser spacings and relatively thick silicon flakes. Finally, at the thermal center of the casting very narrow interlamellar spacings are found again.

The analysis of the model outcome shows that the heat extraction restriction imposed by the low thermal diffusivity of the sand mold produces changes in the internal thermal gradients acting in the different positions of the casting. This in turn regulates the energy exchanges of the local regions of the casting and controls the local solidification kinetics. As a result of this situation the operating conditions during local solidification are different in different positions of the casting.


### Acknowledgment

The authors would like to acknowledge the DGAPA, UNAM, for the financial support (Project IN501596) and I. Beltran Piña and C. Atlatenco T. for their valuable technical assistance.


### References


1. D.M. Stefanescu, Methodologies for Modeling of Solidification Microstructure and Capabilities, *ISIJ Int.*, Vol 35 (No. 6), 1995, p 637-650
2. L. Nastac, and D.M. Stefanescu, Macro Transport-Solidification Kinetics Modeling of Equiaxed Dendritic Growth: Part 1 Model Development and Discussion, *Metall. Mater. Trans. A*, Vol 27, 1996, p 4061-4083
3. T. Kraft and H.E. Exner, Numerical Simulation of Solidification. Part 1 : Microsegregation in Binary Alloys, *Z. Metallkde.*, Vol 87 (No. 7), 1996, p 508-611
4. G. Upadhya and A.J. Paul, Solidification Modeling: A Phenomenological Review, *AFS Trans.*, Vol 102, 1994, p 69-80
5. E. Fras and W. Kapturckiewicz, Numerical Simulation and Fourier Thermal Analysis of Solidification Kinetics in High Carbon Fe-C Alloys, *Metall. Mater. Trans. B*, Vol 28B, 1997, p 115-123
6. E. Fras and W. Kapturckiewicz Secondary Nucleation of Eutectic Graphite Grains, *AFS Trans.*, Vol 104, 1996, p 1-4
7. E. Fras and W. Kapturckiewicz, A New Concept in Thermal Analysis of Castings, *AFS Trans.*, Vol 101, 1993, p 505-510

8. E. Fras, Macro and Micro Modeling of the Solidification Kinetics of Castings, *AFS Trans.*, Vol 100, 1992, p 583-591
9. D.M. Stefanescu, Heat Transfer Solidification Kinetics Modeling of Solidification of Castings, *Metall. Trans. A*, Vol 21, 1990, p 997-1006
10. D. Goettsch and J. Dantzig, Modeling Microstructure Development in Gray Irons, *Metall. Mater. Trans. A*, Vol 25, 1994, p 1063-1079
11. R. Sasikumar and M. Kumar, The Strength of the Coupling between Macroscopic Heat Flow and Equiaxed Grain Formation in Castings, *Acta Metall. Mater.*, Vol 43 (No. 12), 1995, p 4387-4392
12. S. Gowri and F.H. Samuel, Effect of Cooling Rate on the Solidification Behaviour of Al-7Pct Si-SiCp Metal-Matrix Composites, *Metall.. Trans. A*, Vol 23, 1992, p 3369-3376
13. P. Magnin, Eutectic Growth: A Modification of the Jackson and Hunt Theory, *Acta Metall. Mater.*, Vol 39 (No. 4), 1991, p 453-467
14. P. Magnin, Growth of Irregular Eutectics and the Al-Si System, *Acta Metall. Mater.*, Vol 39 (No. 4), 1991, p 469-480
15. E. Fras and W. Kapturckiewicz, Computer Modeling of Fine Graphite Eutectic Grain Formation in the Casting Central Part, Modeling of Casting, *Welding and Advanced Solidification Processes VI*, T.S. Piwonka. Ed., The Minerals, Metals and Materials Society (TMS), 1993, p 261-268
16. M. Flemings, *Solidification Processing*, McGraw-Hill, 1974, p 5-12